Journal of Biomechanics 184 (2025) 112669

Contents lists available at ScienceDirect

Journal of Biomechanics

journal homepage: www.elsevier.com/locate/jbiomech

Effects of nucleotomy on segmental flexibility: A numerical analysis

Maxim Bashkuev [a], Hendrik Schmidt [a,*], Sara Checa [a,b], Sandra Reitmaier [a]

[a] Julius Wolff Institute, Berlin Institute of Health at Charité – Universitätsmedizin, Berlin, Germany
[b] Hamburg University of Technology, Institute of Biomechanics, Hamburg, Germany

ARTICLE INFO

Keywords:
Nucleotomy
Bone healing
Bone remodeling
Stability
Ovine
Intervertebral disc
Lumbar spine

ABSTRACT

Nucleotomy, a common treatment for disc herniations, aims to relieve pressure on spinal structures. While effective in alleviating symptoms, this intervention can compromise spinal stability. However, previous *in vivo* studies in sheep have demonstrated conflicting results with significant long-term stiffening of the spine following nucleotomy, with occasional spontaneous fusion of the affected motion segment. The objective of this study was to investigate the mechanical regulation of tissue adaptation processes post-nucleotomy using computational modeling.

A parametric finite element model of the L4–L5 ovine spinal motion segment, developed previously, was modified to simulate surgical procedures that have been performed in prior *in vivo* studies. An iterative approach was used to simulate post-surgical tissue healing and adaptation processes. Two loading scenarios were simulated: one with combined axial compression and flexion moments, and the other incorporating axial rotation.

An initial decrease in stability, with stiffness reduced by up to 50% due to disc decompression and nucleus removal, was followed by a gradual increase in stiffness over time as a consequence of bone healing and remodeling, with the most pronounced stiffening – up to 350% of the intact state – observed in axial rotation. The findings align with previous *in vivo* observations, suggesting that spontaneous fusion and increased rigidity may be natural consequences of mechano-biological adaptation.

The results of this study highlight that healing processes accompanied by adaptive bone remodeling are directed towards restoration of spinal stability after nucleotomy. These findings align with previous *in vivo* observations, suggesting that spontaneous fusion and increased rigidity may be a natural consequence of post-nucleotomy mechano-biological adaptation. On the other hand, the results indicate a critical role of an appropriate loading regime on the outcome of these processes.

1. Introduction

Nucleotomy, a common surgery for lumbar disc herniations with radiculopathy (Kanno et al., 2019; Kreiner et al., 2014), involves partial removal of the nucleus pulposus through an incision in the annulus fibrosus to decompress neural structures and alleviate symptoms. However, this removal of disc material can compromise spinal stability, a key factor implicated in the development of low back pain (Panjabi, 2003). Alone the annular disruption can result in an immediate reduction in spinal stiffness (Michalek et al., 2010; Michalek and Iatridis, 2012), while removal of nucleus material amplifies the effect (Zöllner et al., 2000). Both annular injury and disc height reduction potentially accelerate degeneration (Inoue and Espinoza Orías, 2011; Vergroesen et al., 2015), further contributing to spinal instability (Fujiwara et al., 2000; Kirkaldy-Willis and Farfan, 1982).

In vitro studies show an immediate increase in flexibility (Burkhard et al., 2023; Reitmaier et al., 2014), yet *in vivo* findings are less consistent. Specifically, while *in vitro* studies consistently report an immediate increase in segmental flexibility following nucleotomy, the long-term outcomes vary, with some studies observing significant stiffening and even spontaneous fusion of the motion segment (Reitmaier et al., 2014). Long term clinical studies reported reduced flexibility (Halldin et al., 2005) or an increased likelihood to require a fusion surgery (Castillo et al., 2019), compared to patients who did not undergo the procedure. This suggests an elevated risk of instability after nucleotomy, underscoring the growing popularity of spinal fusion as a treatment of instability (Lambrechts et al., 2022; Makanji et al., 2018). Conversely, long-term animal studies (Reitmaier et al., 2017, 2014) have shown substantial stiffening of the affected spinal segments, with some cases of spontaneous bony fusion observed six months post-operatively, even

* Corresponding author at: Julius Wolff Institute, Berlin Institute of Health at Charité – Universitätsmedizin Berlin, Augustenburger Platz 1, 13353 Berlin, Germany.
E-mail address: hendrik.schmidt@bih-charite.de (H. Schmidt).

https://doi.org/10.1016/j.jbiomech.2025.112669
Accepted 27 March 2025
Available online 29 March 2025

without instrumentation.

This apparent discrepancy between short-term instability and long-term stiffening suggests the involvement of adaptive processes within the spine, compensating for the altered mechanical environment post-surgery. To better understand these processes, the present study employs computational modelling to investigate the mechanical regulation of tissue healing and adaptation following nucleotomy in an ovine lumbar spinal segment.

We hypothesized that the post-surgical mechanical stimuli are within those previously reported to stimulate a bone formation response, hence promoting a gradual restoration of stability in the affected motion segment. This study aims to quantify how adaptive processes contribute to the restoration of spinal stability following nucleotomy, thereby addressing the discrepancies observed in animal experiments.

2. Methods

To simulate bone remodeling and post-surgical healing, an iterative algorithm, adapted from a prior study by our group (Calvo-Echenique et al., 2019), was implemented in Python (Fig. 1). This algorithm utilizes a finite element model to calculate mechanical stimuli as the basis for the remodeling process. The simulations were conducted over 100 iterations, each representing approximately one day of physiological response. The initial state of the model was established through a preliminary bone remodeling simulation, continued until the bone distribution within the vertebral bodies reached equilibrium.

2.1. Finite element (FE) model

We used a previously developed (Bashkuev et al., 2019) parametric FE model of a lumbar motion segment (Fig. 2a), that enables geometric morphing between human and ovine lumbar segments by adjusting specific parameter values. For the present study, an intact ovine L4-L5 motion segment model was generated using a parameter set comprising mean values sourced from the literature (Mageed et al., 2013; O'Connell et al., 2007).

The model includes vertebral bodies (cortical and cancellous bone and bony endplates), posterior structures (pedicles, transverse and spinous processes, and facet joints), and the intervertebral disc with seven ligaments: anterior and posterior longitudinal ligaments, intertransverse, interspinous and supraspinous ligaments, ligamentum flavum, and facet joint capsules. The intervertebral disc was further divided into cartilaginous endplates, nucleus pulposus, and annulus fibrosus. The latter included twelve concentric layers of collagen fibers embedded within the ground substance. The cross-sectional areas of the fibers were calculated assuming a fiber volume fraction of 16% (Galante, 1967). Ligament cross-sectional areas were scaled from available human specimen data (Pintar et al., 1992) by a factor of 0.5, reflecting the approximate size ratio between human and ovine geometries. The nonlinear stress–strain properties of the ligaments and the annulus fibers were modeled as Marlow hyperelastic model based on uniaxial tensile test data (Schmidt et al., 2007, Schmidt et al.,2006). The annulus fibers were arranged in a crisscross pattern and their orientation relative to the disc transverse plane increased linearly from ±30° in the outermost to ±45° in the innermost layer according to literature (Cassidy et al., 1989;

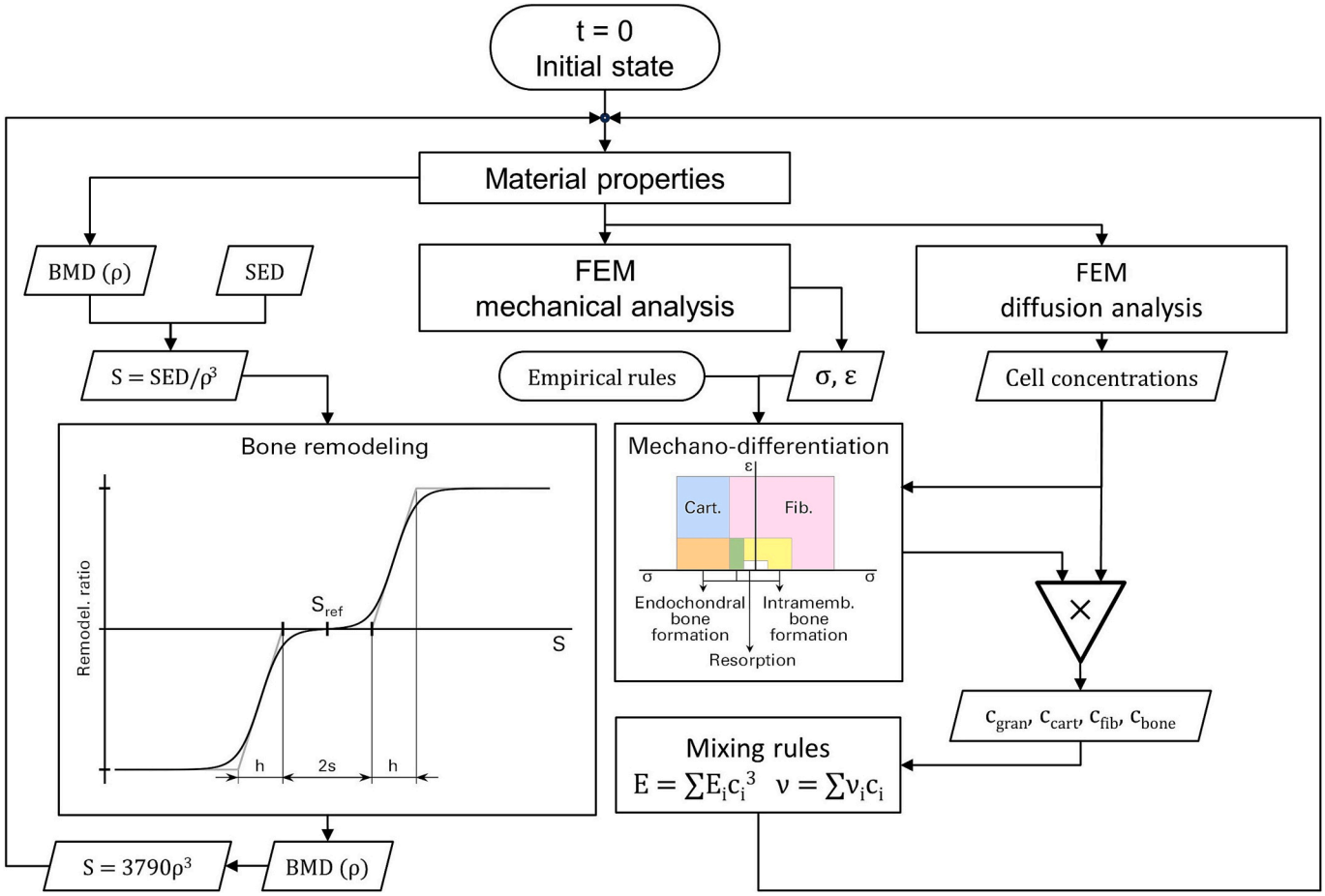

Fig. 1. Flow chart of the implemented iterative process split into adaptive bone remodeling utilizing algorithm of Huiskes et al., (1987), and the mechano-differentiation part adapted from Claes and Heigele (1999) to model new bone formation. For bone remodeling, the relationship between the mechanical stimulus S and remodeling rate was modeled as a double sigmoid function (black line) fitted to the piecewise linear function (equation (2), thin gray line).

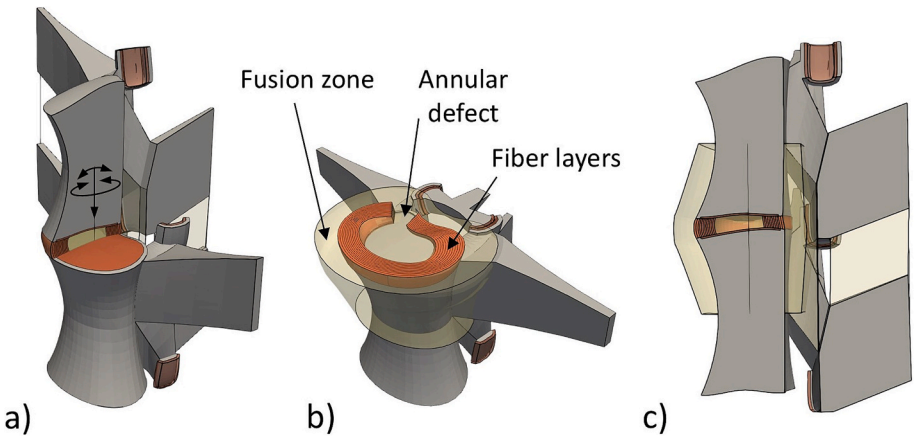

Fig. 2. Finite element model of an ovine L4-L5 motion segment (a). Nucleotomy was modeled to mimic the side access through the annulus as it was done in the experiments (b). 5-mm-thick fusion zone was modeled around the disc, allowing for new bone formation in this region (b-c).

Holzapfel et al., 2005). The mechanical behavior of the model was validated in the previous parametric study (Bashkuev et al., 2019). The interaction of articulating facet surfaces was modeled as frictionless surface-to-surface contact using nonlinear penalty method.

Nucleotomy was modeled using a lateral approach (Fig. 2b), per Reitmaier et al. (2014). Two additional models were generated, with disc height reduced to 75% and 50% of the intact disc height, respectively, to account for post-nucleotomy disc height loss.

2.2. Adaptive bone remodeling algorithm

Bone remodeling in the vertebral bodies after surgery was implemented using an adaptive approach (Fig. 1, left side) similar to the one proposed by Huiskes et al. (1987). The rate of change in bone mineral density (BMD) ρ (g/cm^3) of the vertebrae was regulated by a ratio of the actual to the reference mechanical stimulus. A cubic relationship between BMD and Young's modulus E (MPa) was employed according to Carter and Hayes (1977):

$$E = 3790\rho^3 \tag{1}$$

The original algorithm used the strain energy density (SED) as the driving mechanical stimulus, and a tri-linear bone remodeling rate (with a "lazy" zone around the reference value) (Huiskes et al., 1987). In the previous study, this relationship was extended by adding an upper limit to the remodeling rate (Calvo-Echenique et al., 2019), due to the fact that the stimulus itself is limited by mechanical strength (Beaupré et al., 1990) leading to the following definition:

$$\dot{\rho} = \frac{d}{dt}\rho = \begin{cases} R(1+s+h), & S^i \geq (1+s+h)S^{ref} \\ R\left(\dfrac{S^i}{S^{ref}} - (1+s)\right), & (1+s+h)S^{ref} > S^i > (1+s)S^{ref} \\ 0, & (1+s)S^{ref} \geq S^i \geq (1-s)S^{ref} \\ R\left(\dfrac{S^i}{S^{ref}} - (1-s)\right), & (1-s)S^{ref} > S^i > (1-s-h)S^{ref} \\ R(1-s-h), & S^i \leq (1-s-h)S^{ref} \end{cases} \tag{2}$$

where the remodeling rate remains zero within the "lazy zone" with the width of 2 s centered at S^{ref} and increases or decreases linearly outside of it; h is the width of the zones with positive slope R. The relationship (2) between mechanical stimulus and remodeling rate was in the current study replaced by a continuous equivalent, defined as a sum of two logistic sigmoid (expit) functions:

$$\dot{\rho} = \frac{d}{dt}\rho = \dot{\rho}_{max}(expit(k(x-s)) - expit(-k(x+s)))$$
$$x = \frac{S_i}{S_{ref}} - 1 \tag{3}$$

The parameters $\dot{\rho}_{max}$ and k can be calculated from the parameters R, s and h from the equation (3) so, that both functions are maximally close (Fig. 1).

The stimulus S was defined as the ratio of SED to the cube of ρ (4) instead of the SED value used in the original algorithm, to avoid numerical instabilities described by Weinans et al., (1992):

$$S = \frac{SED}{\rho^3} \tag{4}$$

To investigate the performance of the algorithm, an intact model (without surgical interventions) was simulated starting from a uniform BMD distribution of 0.1 g/cm^3 and the algorithm was run until BMD reached equilibrium. The lower and upper limits of BMD were set to 0.01 and 1.74 g/cm^3, beyond which no further decrease or increase, respectively, was allowed. The lower limit represented complete bone resorption and the upper corresponded to the Young's modulus of 20 GPa, which was assumed to be the Young's modulus of cortical bone.

2.3. Bone formation algorithm

In the nucleotomy models, the regions from where intact tissues were removed during the intervention (nucleus, cartilage endplates and the annulus incision) as well as a 5-mm-wide region around the segment were replaced with granulation tissue (Fig. 2b-c). These regions were assumed eligible for progenitor cell migration from the bone marrow, which was modeled as a diffusive process, with $\frac{dn}{dt} = D \cdot \nabla^2 n$, where the cell density n is determined from the diffusion coefficient D, which was specifically chosen so that the whole intervertebral space was saturated after 28 iterations (Bashkuev et al., 2015; Hsu et al., 2018). The source of the cells was assumed as constant concentration on the adjacent endplate surfaces, and the cell concentration was normalized to 1. The mechanical stimuli (distortional equivalent strain and hydrostatic strain, equations (5) and (6) were calculated in each iteration according to the mechano-regulation rules adapted from Claes and Heigele (1999):

$$\varepsilon_d = \frac{2}{3}\sqrt{\left[(\varepsilon_1-\varepsilon_2)^2 + (\varepsilon_2-\varepsilon_3)^2 + (\varepsilon_1-\varepsilon_3)^2\right]} \tag{5}$$

$$\varepsilon_h = \frac{1}{3}tr\left(\underline{\underline{\varepsilon}}\right) \tag{6}$$

Where ε_1, ε_2 and ε_3 are principal strains and $tr(\underline{\varepsilon})$ is trace of the strain tensor. The threshold values of ±1% for hydrostatic strain and 5% for equivalent strain were used for bone formation. The resorption limits were set to 0.1% and 1% for the hydrostatic strain and the equivalent strain, respectively (Postigo et al., 2014). Based on the mechanical stimulus, the precursor cells could differentiate into fibroblasts, chondrocytes, or osteoblasts; the exact conditions for the tissue differentiation along with the additional empirical rules were taken from the previous study (Calvo-Echenique et al., 2019). In turn, cartilage could also change to bone during endochondral ossification and fibrous tissue could morph into cartilage. The precursor cells, chondroblasts, and fibroblasts were allowed to differentiate by a maximum of 0.1, 0.1 and 0.2 per iteration, respectively, while the resorption rate was limited to 0.05/iteration to avoid instabilities (Isaksson et al., 2008). For each element, the Young's modulus (E) was calculated as a weighted sum of the Young's moduli of each tissue type present in the element depending on the cube of their volumetric fractions (7), according to Carter and Hayes (1977). Poisson's ratio ν was calculated in a similar way using first order of volumetric fractions (Shefelbine et al., 2005):

$$\begin{cases} E = \sum E_i {c_i}^3 \\ \nu = \sum \nu_i c_i \\ i \in [gran, fib, cart, bone] \end{cases} \quad (7)$$

where c_{gran}, c_{fib}, c_{cart}, and c_{bone} are the volumetric fractions of granular tissue, fibrous tissue, cartilage, and bone, respectively.

It was assumed that new bone formation only occurs on the surfaces of existing bone (in the initial fusion phase at the vertebral surface), similar to the fracture-healing processes (Claes and Heigele, 1999; Uhthoff and Rahn, 1981). Therefore, bone apposition was allowed when the concentration of bone in a neighboring element exceeded 0.25.

For nucleotomy models, rotational stiffness was compared to the experimental data. Due to high value ranges found in the experiments (Reitmaier et al., 2017), the values were normalized to the intact state, which was set to 100%.

2.4. Boundary and loading conditions

While knowledge of the axial rotation in ovine lumbar spine *in vivo* is lacking, the orientation of the facet joints at the lumbar level suggests that axial loading should be fairly limited. On the other hand, torsion is known to affect both bone healing (Mølster, 1984; Steiner et al., 2014) and remodeling (Carpenter and Carter, 2008; Levenston et al., 1998). Therefore, two loading scenarios were simulated in this study – one involved a combination of axial compression and flexion/extension moments, while the other additionally included axial rotation. Lateral bending was not included in the simulations due to its weak correlation with intradiscal pressure, making it challenging to estimate accurately based on available literature data. The load was applied incrementally: first, an axial compression of 160 N was applied, followed by an increase to 220 N. In the subsequent step, a flexion moment of 2.2 Nm was applied. The second loading scenario included two additional steps – axial rotation of 2.2 Nm to the left and right. The load magnitudes were selected to represent moderate physiological loading (Hauerstock et al., 2001; Reitmaier et al., 2013). In total, six nucleotomy simulations that incorporated both healing and remodeling (at 50%, 75%, and 100% of intact disc height under two loading conditions) have been performed.

The compressive load was applied as follower load using a two-node connector element to mitigate the introduction of additional bending moments. The nodes of the connector were constrained to the distal endplates of the corresponding vertebrae through a multi-point constraint. The lower endplate of the inferior vertebra was rigidly fixed by restricting all degrees of freedom at the lower node of the connector element. The application point for the flexion/extension and axial rotation moments was located at the upper node of the connector element.

The mechanical stimuli values were computed as the weighted average of the respective values during each loading step, with weights assumed as follows: 0.25 for the first compression step, 0.5 for the second compression step, and 0.25 for the combined loading step. This weighting approximates the daily activity patterns observed in sheep (Reitmaier et al., 2013).

Mesh refinement was conducted in a prior study (Bashkuev et al., 2019) under a 160 N compressive load followed by a 3.75 Nm flexion/extension moment, ensuring that the differences in predicted stress distributions between two consecutive mesh densities were less than 5%. Finite element simulations were carried out using commercial FE software ABAQUS 6.14 (Simulia, Providence, RI, USA).

3. Results

3.1. Bone remodeling in the intact model

The simulation started with a uniform BMD of 0.1 g/cm^3. In the initial iteration, the remodeling rate within both vertebral bodies was at its peak. During the first 25 iterations, BMD in the unloaded transverse and spinous processes, as well as in the inferior facets of the lower vertebra, declined to the lower limit of 0.01 g/cm^3, indicating complete resorption. By the 50th iteration, BMD in the cancellous bone of the vertebral bodies reached equilibrium, while the cortical shell continued to develop up to approximately 100 iterations. Notably, BMD in the anterior regions of the cortical shell reached the maximum of 1.74 g/cm^3, however, the remodeling stimulus remained elevated. Additionally, the distal endplates did completely resorb, similar to the transverse processes. The BMD of the articulating facet joints reached its maximum value within the first 25 iterations and subsequently stabilized (Fig. 3b).

3.2. Bone healing and overall stiffness recovery

The nucleotomy models did not achieve solid bony consolidation. However, all models predicted partial fusion, resulting in osteophyte-like formations in the fusion region outside the intervertebral space (Fig. 4). The annulus defect played a critical role in facilitating bone formation beyond the nucleus cavity, as it provided a pathway for precursor cells to migrate outward, thereby serving as the initial site of bone formation. In contrast to typical bone remodeling processes, none of the pure nucleotomy models reached an equilibrium state in terms of bone distribution patterns.

Flexional stiffness stabilized after 20 iterations in models with 100% and 75% disc height, while lateral bone formation progressed beyond 100 iterations, continuously increasing torsional stiffness. Under load combinations involving axial rotation, the distortional strain in the outer periphery was excessively high, inhibiting further bone formation in the outer fusion region. Conversely, in the initial loading scenario without rotation, the mechanical stimulus effectively promoted the formation of relatively large volumes of new bony tissue. Notably, osteophyte-like bone developed laterally in the outer periphery, bridging the gap after approximately 30 iterations, resulting in a significantly higher torsional stiffness (Fig. 5).

Flexibility tests of the final configuration (after 100 iterations) under isolated pure moments, similar to those conducted in the experiments, revealed different patterns based on the modeled disc height loss and loading scenario (Fig. 6). In all investigated models, the final stiffness at 2.2 Nm exceeded that of the intact model. Models subjected to the loading scenario without rotation produced a greater volume of newly formed bone in the outer periphery, resulting in a considerably stiffer and nearly linear response, whereas the other cases retained a slight nonlinearity. In axial compression, all models, including the intact one, were generally too compliant compared to the experiments (Fig. 6).

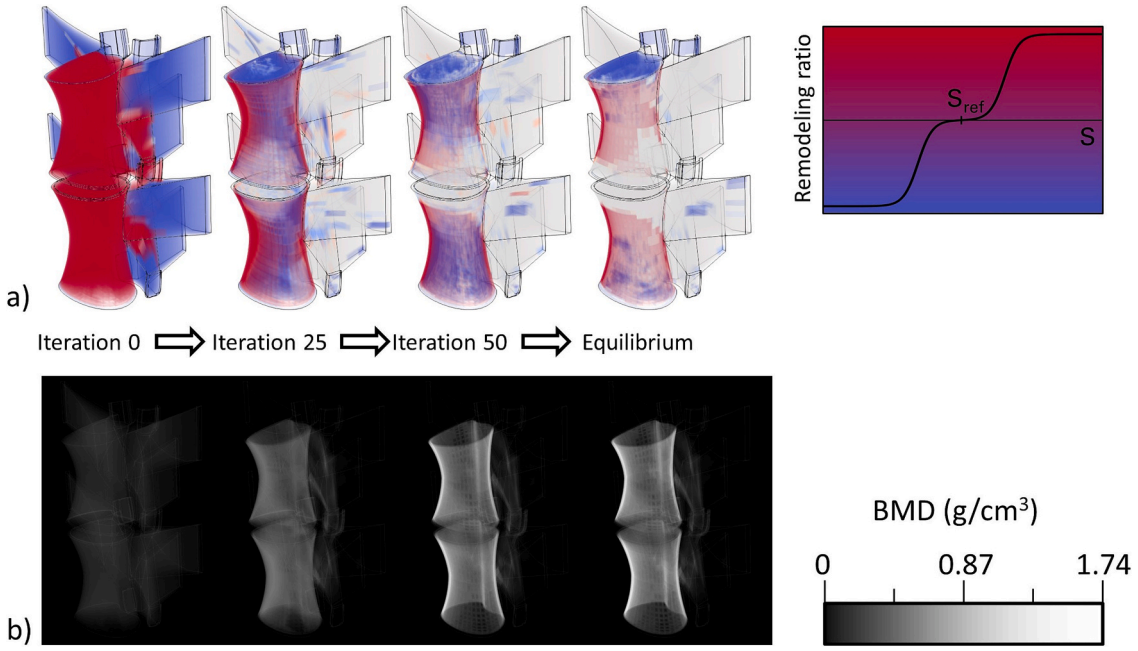

Fig. 3. Remodeling of the intact model starting with a low, uniformly distributed bone density shows high remodeling rate at start of the simulation, which continuously decreases until bone remodeling and resorption reach equilibrium (a) and a sequence of virtual "X-ray" images indicating restoration of the intact configuration of bony elements (b).

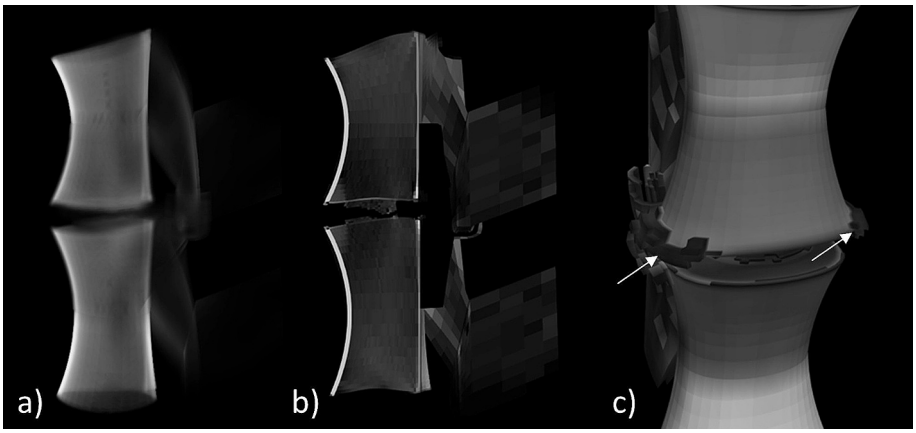

Fig. 4. (a) Simulated X-ray image of a failed fusion in the nucleotomy model with 100% disc height. (b) Mid-plane cut through the model showing the predicted non-union within the disc space as well as the adapted bone distribution within the vertebral bodies. (c) Osteophyte-like bone formations (arrows) predicted at the outer periphery of the disc.

4. Discussion

The present study aimed to investigate the experimentally observed increase in stability after a nucleotomy, using an iterative mechano-regulation computer model. Simulations demonstrated that mechanically driven tissue healing and adaptation responses to the surgical intervention can explain the experimentally observed increase in stability after nucleotomy.

Modern spinal fusion techniques primary achieve stabilization through the use of devices such as interbody cage or internal fixators (Mobbs et al., 2015). In contrast, the pioneering spinal fusion technique developed by Hibbs involved the placement of a bone graft between the pedicles, relying solely on biological processes for stabilization (Tarpada et al., 2017). Recently, an experimental *in vivo* study conducted by Reitmaier et al. (2017) demonstrated successful spinal fusion without instrumentation following nucleotomy in sheep. This finding suggests that natural adaptive mechanisms can effectively restore stability lost due to surgical intervention.

Adaptation is a complex process involving bone remodeling, new bone formation, and likely soft tissue changes. Reitmaier et al. (2017) postulated that aggressive nucleotomy could serve as a potent catalyst for new bone formation hypothesizing that access to the vertebral vascular network beneath the subchondral bone of the endplates would provide essential progenitor cells, cytokines, and nutrients necessary for effective healing, while the increased flexibility resulting from nucleotomy may create a favorable mechanical stimulus to promote tissue healing and adaptation (Halvachizadeh and Pape, 2020). Our computer model simulations predicted a bone formation response confirming this hypothesis. Previous studies have shown that the mechanical regulation of bone healing can explain the fusion process in spinal fusion treated with cages and fixators (Calvo-Echenique et al., 2019; Postigo et al., 2014). In this study, our simulations have shown that the lack of a cage leads to the loss of initial stability and, thus, to excessive mechanical stimulus which resulted in non-union. Nonetheless, the models

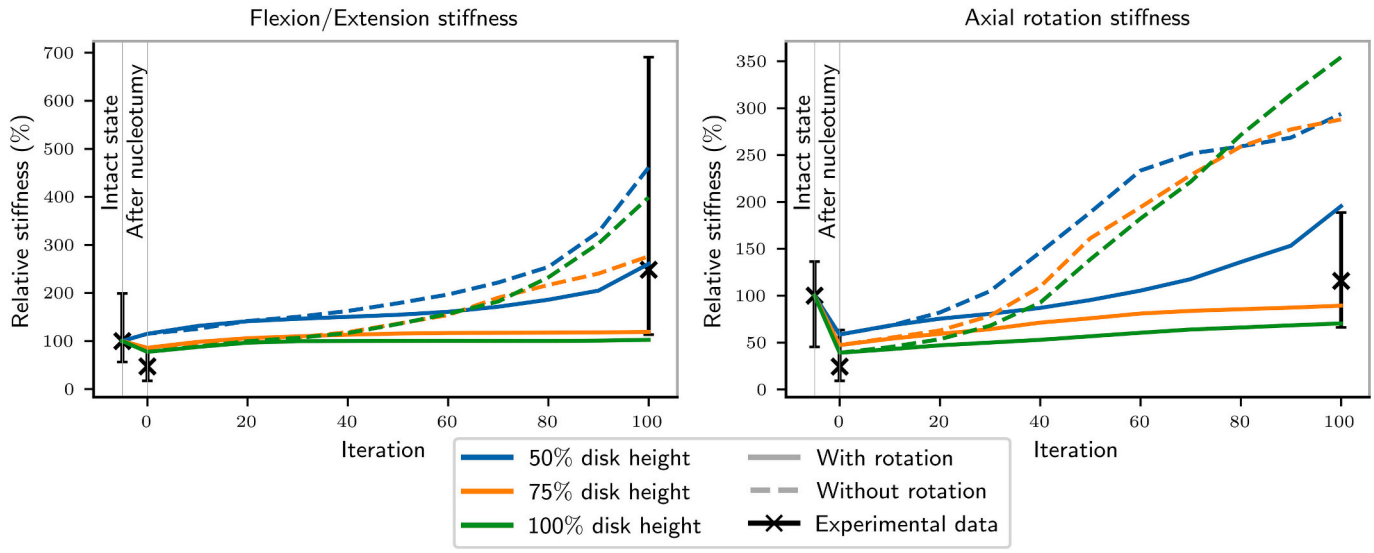

Fig. 5. Temporal variation of the flexion/extension (a) and torsional stiffness (b) relative to the initial state for the nucleotomy models under both loading scenarios.

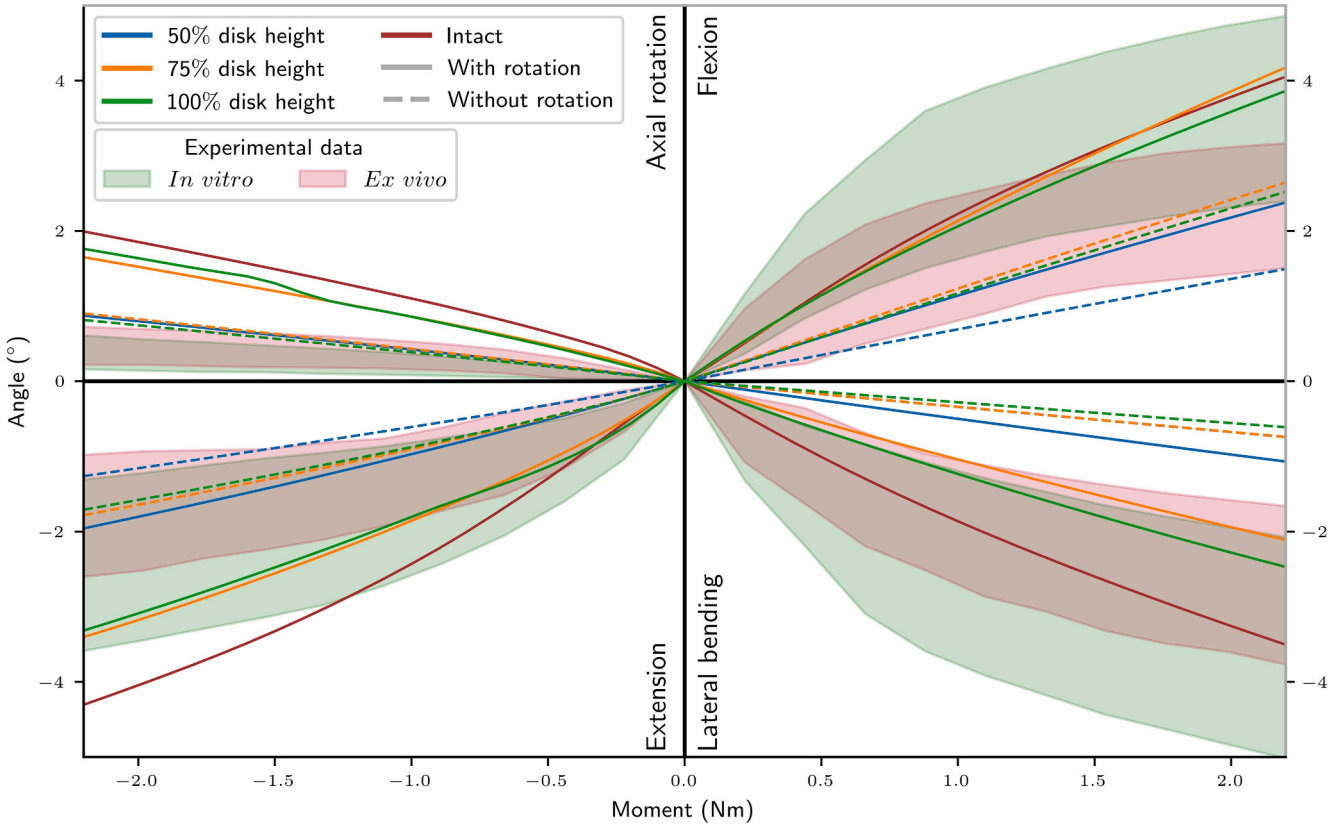

Fig. 6. Resulting moment–angle curves at the end of the simulations in comparison to the intact state and experimental data. Green areas show stiffness ranges from intact specimens measured *in vitro*; *ex vivo* corresponds to the specimens extracted from animals sacrificed 12 weeks after surgery. Note that the dashed line of 50% is hidden behind that of 75% in lateral bending.

predicted the restoration of the stability of the affected segment over time reaching pre-operation levels.

In addition to biological and genetic factors, the mechanical environment substantially influences the structural adaptation of bone. According to the "three-joint complex" principle proposed by Kirkaldy-Willis et al. (1978), nucleotomy alters load sharing between the anterior and posterior columns, consequently affecting the force transmission within the vertebral bodies. In this study, we showed that nucleotomy leads to a change in the mechanical environment within the vertebral bodies that, according to the current principles of bone remodeling, leads to a bone adaptation response.

As verification of the bone remodeling component, we conducted a simulation on an intact model devoid of injury or instrumentation, beginning with a uniformly low bone density assigned to all bony elements throughout the vertebral bodies. The complex architecture of the spine *in vivo* is shaped through centuries of evolution and likely

programmed by genetic factors; therefore, we determined the reference mechanical stimulus S^{ref} for individual elements, based on the intact model. The model was expected to restore its bone structure to the reference state. However, during the simulation, certain regions of the posterior elements failed to restore their bone density, resulting in complete resorption. This outcome was anticipated, given that the primary loading condition was compression. Under compressive loads, the tensile ligaments played a negligible role in load sharing; as a result, the load was predominantly transferred to the intervertebral disc and facet joints: Consequently, the transverse and spinous processes, which were not involved in load transmission, did not receive the mechanical stimuli necessary to maintain their bone structure. This is similar to the effects of microgravity observed in spaceflight and hindlimb unloading experiments *in vivo* (Nagaraja and Risin, 2013).

Generally, stress-driven bone remodeling models exhibit a positive feedback loop that can lead to divergent solutions, as mathematically demonstrated by Weinans et al., (1992). They also noted that the adaptive bone remodeling algorithm originally proposed by Huiskes et al., (1987) converges to a stable solution only when the absolute value γ of the relationship $E = c\rho^{\gamma}$ is less than 1. To circumvent this issue, we divided SED by ρ^3 and used this ratio as the stimulus, rather than relying solely on SED. This approach effectively transformed the model into a strain-driven solution. The resulting remodeling algorithm produced regions with a smooth and uniform distribution of bone density.

All nucleotomy models (with disc heights of 50%, 75% and 100%) predicted some bone material within the remaining intervertebral space and at the outer periphery of the intended fusion zone. Although solid bony consolidation was not achieved in any of the models, stiffness tests indicated a consistent progression of the fusion process, agreeing with experimental observations. The results of the simulations indicate that the extent of disc height loss following nucleotomy significantly influences the final stiffness outcomes, with greater height loss leading to different patterns of bone formation and stiffness recovery. This underscores the importance of accurately measuring or estimating post-nucleotomy disc height in both experimental and clinical settings to better understand and predict long-term outcomes. Regarding the increase in stiffness over time, both experimental and the simulation results exhibited a wide range of values, complicating the ability to draw definitive conclusions about how closely the simulations resemble the *in vivo* conditions observed in animal experiments. In terms of the resulting stiffness curves, none of the models aligned perfectly with the experimental data across all loading directions. In general, in all movement directions, the models predicted a strong recovery of the segment stability, reaching stiffness values exceeding the intact spine, when rotation loading conditions were not taken into account. Experimentally, nucleotomy led to a loss of mechanical stability immediately after surgery, which was then recovered to values close to the intact situation.

The present study has several limitations that should be considered when interpreting the findings. Neglecting lateral bending, due to lack of experimental data and its weak correlation with intradiscal pressure, may limit the representation of daily loading. In contrast to humans, sheep generally exhibit higher rates of bone turnover and remodeling, characterized by distinct seasonal variations (Arens et al., 2007; Bonucci and Ballanti, 2014; Pearce et al., 2007). These factors were not considered in the present model and the present results indicate that the algorithm might require further calibration. The remodeling part of the algorithm employed the power law relationship between BMD and Young's modulus derived from human and bovine trabecular bone (Carter and Hayes, 1977). While this relationship is generally accepted and is consistent across species (Currey, 1988; Helgason et al., 2008), the specific parameters may vary for ovine vertebral bone. To address this uncertainty, we constrained the maximum BMD to correspond to the Young's modulus of ovine cortical bone. The remodeling simulation of the intact segment successfully restored the bone distribution (Fig. 3), supporting the validity of our approach. The remodeling algorithm did not account for ligamentous ossification, which may have led to the inability to reproduce some experimental results. However, some models exhibited similar patterns with the formation of thin osteophyte-like bone bridges external to the annulus ring. The employed mechano-differentiation algorithm was originally developed and calibrated for long bone healing (Claes and Heigele, 1999) and subsequently adapted for spinal fusion simulations in human models (Calvo-Echenique et al., 2019). However, bone healing processes are comparable in sheep and human (Malhotra et al., 2014), therefore we assumed the application of the algorithm to be reasonable. In the animal experiments conducted by Reitmaier et al. (2017, 2014), the animals were euthanized after twelve weeks and six months, resulting in experimental data represent "snapshots" from different specimens at various time points. Consequently, continuous measurements of stiffness were not available to validate the stiffness progression or calibrate the model parameters in the current simulations. Finally, there was no imaging material available that was suited for validating the implemented bone remodeling algorithm.

While validation of the healing models poses significant challenges and is not always feasible, the present simulations indicate that achieving stabilization through nucleotomy without instrumentation is a mechanically viable scenario. The bone healing algorithm predicted new bone formation that effectively countered the substantial decrease in model stiffness resulting from the removal of nucleus material during nucleotomy. For all loading conditions and boundary constraints, the initial loss of stability following nucleotomy could be fully recovered throughout the simulations.

In conclusion, the present study indicates that the increase in stability following nucleotomy without instrumentation can be explained by the mechano-regulation of tissue healing responses. The computer framework developed in this study could in the future be used to support the design of pre-clinical studies or inform surgical approaches.

CRediT authorship contribution statement

Maxim Bashkuev: Writing – review & editing, Writing – original draft, Visualization, Validation, Software, Methodology, Investigation, Formal analysis, Data curation, Conceptualization. **Hendrik Schmidt:** Writing – review & editing, Supervision, Resources, Project administration, Funding acquisition, Conceptualization. **Sara Checa:** Writing – review & editing, Validation, Supervision, Methodology, Funding acquisition. **Sandra Reitmaier:** Writing – review & editing, Supervision, Resources, Investigation, Funding acquisition, Conceptualization.

Declaration of competing interest

The authors declare that they have no known competing financial interests or personal relationships that could have appeared to influence the work reported in this paper.

Acknowledgments

This study is part of the Research Unit FOR 5177 funded by the German Research Foundation (RE 4292/3-1, CH 1123/9-1, SCHM 2572/12-1).

References

Arens, D., Sigrist, I., Alini, M., Schawalder, P., Schneider, E., Egermann, M., 2007. Seasonal changes in bone metabolism in sheep. Vet. J. 174, 585–591. https://doi.org/10.1016/j.tvjl.2006.10.001.

Bashkuev, M., Checa, S., Postigo, S., Duda, G., Schmidt, H., 2015. Computational analyses of different intervertebral cages for lumbar spinal fusion. J. Biomech. 48, 3274–3282. https://doi.org/10.1016/j.jbiomech.2015.06.024.

Bashkuev, M., Reitmaier, S., Schmidt, H., 2019. Is the sheep a suitable model to study the mechanical alterations of disc degeneration in humans? A probabilistic finite element model study. J. Biomech. 84, 172–182. https://doi.org/10.1016/j.jbiomech.2018.12.042.

Beaupré, G.S., Orr, T.E., Carter, D.R., 1990. An approach for time-dependent bone modeling and remodeling-application: a preliminary remodeling simulation. J. Orthop. Res. 8, 662–670. https://doi.org/10.1002/jor.1100080507.

Bonucci, E., Ballanti, P., 2014. Osteoporosis—Bone Remodeling and Animal Models. Toxicol. Pathol. 42, 957–969. https://doi.org/10.1177/0192623313512428.
Burkhard, M.D., Calek, A.K., Fasser, M.R., Cornaz, F., Widmer, J., Spirig, J.M., Wanivenhaus, F., Farshad, M., 2023. Biomechanics after spinal decompression and posterior instrumentation. Eur. Spine J. 32, 1876–1886. https://doi.org/10.1007/s00586-023-07694-5.
Calvo-Echenique, A., Bashkuev, M., Reitmaier, S., Pérez-del Palomar, A., Schmidt, H., 2019. Numerical simulations of bone remodelling and formation following nucleotomy. J. Biomech. 88, 138–147. https://doi.org/10.1016/j.jbiomech.2019.03.034.
Carpenter, R.D., Carter, D.R., 2008. The mechanobiological effects of periosteal surface loads. Biomech. Model. Mechanobiol. 7, 227–242. https://doi.org/10.1007/s10237-007-0087-9.
Carter, D.R., Hayes, W.C., 1977. The compressive behavior of bone as a two-phase porous structure. J. Bone Joint Surg. Am. 59, 954–962.
Cassidy, J.J., Hiltner, A., Baer, E., 1989. Hierarchical structure of the intervertebral disc. Connect. Tissue Res. 23, 75–88.
Castillo, H., Chintapalli, R.T.V., Boyajian, H.H., Cruz, S.A., Morgan, V.K., Shi, L.L., Lee, M.J., 2019. Lumbar discectomy is associated with higher rates of lumbar fusion. Spine J. 19, 487–492. https://doi.org/10.1016/j.spinee.2018.05.016.
Claes, L.E., Heigele, C.A., 1999. Magnitudes of local stress and strain along bony surfaces predict the course and type of fracture healing. J. Biomech. 32, 255–266.
Currey, J.D., 1988. The effect of porosity and mineral content on the Young's modulus of elasticity of compact bone. J. Biomech. 21, 131–139. https://doi.org/10.1016/0021-9290(88)90006-1.
Fujiwara, A., Tamai, K., An, H.S., Kurihashi, A., Lim, T.-H., Yoshida, H., Saotome, K., 2000. The relationship between disc degeneration, facet joint osteoarthritis, and stability of the degenerative lumbar spine. J. Spinal Disord. 13, 444–450. https://doi.org/10.1097/00002517-200010000-00013.
Galante, J.O., 1967. Tensile Properties of the Human Lumbar Annulus Fibrosus. Acta Orthop. Scand. 38, 1–91. https://doi.org/10.3109/ort.1967.38.suppl-100.01.
Halldin, K., Zoëga, B., Nyberg, P., Kärrholm, J., Lind, B.I., 2005. The effect of standard lumbar discectomy on segmental motion: 5-Year follow-up using radiostereometry. Int. Orthop. 29, 83–87. https://doi.org/10.1007/s00264-005-0636-8.
Halvachizadeh, S., Pape, H.-C., 2020. Perren's Strain Theory and Fracture Healing, in: Crist, B.D., Borrelli Jr., J., Harvey, E.J. (Eds.), Essential Biomechanics for Orthopedic Trauma: A Case-Based Guide. Springer International Publishing, Cham, pp. 17–25. Doi: 10.1007/978-3-030-36990-3_2.
Hauerstock, D., Reindl, R., Steffen, T., 2001. Telemetric measurement of compressive loads in the sheep lumbar spine, in: Transactions of the 47th Annual Meeting of The Orthopaedic Research Society. San Francisco, California.
Helgason, B., Perilli, E., Schileo, E., Taddei, F., Brynjólfsson, S., Viceconti, M., 2008. Mathematical relationships between bone density and mechanical properties: A literature review. Clin. Biomech. 23, 135–146. https://doi.org/10.1016/j.clinbiomech.2007.08.024.
Holzapfel, G., Schulze-Bauer, A., Feigl, C., Regitnig, G., 2005. Single lamellar mechanics of the human lumbar anulus fibrosus. Biomech. Model. Mechanobiol. 3, 125–140. https://doi.org/10.1007/s10237-004-0053-8.
Hsu, H.-W., Bashkuev, M., Pumberger, M., Schmidt, H., 2018. Differences in 3D vs. 2D analysis in lumbar spinal fusion simulations. J. Biomech. 72, 262–267. https://doi.org/10.1016/j.jbiomech.2018.03.009.
Huiskes, R., Weinans, H., Grootenboer, H.J., Dalstra, M., Fudala, B., Slooff, T.J., 1987. Adaptive bone-remodeling theory applied to prosthetic-design analysis. J. Biomech. 20, 1135–1150. https://doi.org/10.1016/0021-9290(87)90030-3.
Inoue, N., Espinoza Orías, A.A., 2011. Biomechanics of Intervertebral Disk Degeneration. Orthop. Clin. North Am. 42, 487–499. https://doi.org/10.1016/j.ocl.2011.07.001.
Isaksson, H., van Donkelaar, C.C., Huiskes, R., Ito, K., 2008. A mechano-regulatory bone-healing model incorporating cell-phenotype specific activity. J. Theor. Biol. 252, 230–246. https://doi.org/10.1016/j.jtbi.2008.01.030.
Kanno, H., Aizawa, T., Hahimoto, K., Itoi, E., 2019. Minimally invasive discectomy for lumbar disc herniation: current concepts, surgical techniques, and outcomes. Int. Orthop. 43, 917–922. https://doi.org/10.1007/s00264-018-4256-5.
Kirkaldy-Willis, W.H., Wedge, J.H., Yong-Hing, K., Reilly, J., 1978. Pathology and pathogenesis of lumbar spondylosis and stenosis. Spine (Phila. Pa. 1976). Doi: 10.1097/00007632-197812000-00004.
Kirkaldy-Willis, W.H., Farfan, H.F., 1982. Instability of the lumbar spine. Clin. Orthop. Relat. Res. 10, 110–123.
Kreiner, D.S., Hwang, S.W., Easa, J.E., Resnick, D.K., Baisden, J.L., Bess, S., Cho, C.H., Depalma, M.J., Dougherty, P., Fernand, R., Ghiselli, G., Hanna, A.S., Lamer, T., Lisi, A.J., Mazanec, D.J., Meagher, R.J., Nucci, R.C., Patel, R.D., Sembrano, J.N., Sharma, A.K., Summers, J.T., Taleghani, C.K., Tontz, W.L., Toton, J.F., 2014. An evidence-based clinical guideline for the diagnosis and treatment of lumbar disc herniation with radiculopathy. Spine J. 14, 180–191. https://doi.org/10.1016/j.spinee.2013.08.003.
Lambrechts, M.J., Siegel, N., Heard, J.C., Karamian, B.A., Dambly, J., Baker, S., Brush, P., Fras, S., Canseco, J.A., Kaye, I.D., Woods, B.I., Hilibrand, A.S., Kepler, C.K., Vaccaro, A.R., Schroeder, G.D., 2022. Trends in Single-Level Lumbar Fusions Over the Past Decade Using a National Database. World Neurosurg. 167, e61–e69. https://doi.org/10.1016/j.wneu.2022.07.092.
Levenston, M.E., Beaupré, G.S., Carter, D.R., 1998. Loading mode interactions in simulations of long bone cross-sectional adaptation. Comput. Methods Biomech. Biomed. Engin. 1, 303–319. https://doi.org/10.1080/01495739808936709.
Mageed, M., Berner, D., Jülke, H., Hohaus, C., Brehm, W., Gerlach, K., 2013. Is sheep lumbar spine a suitable alternative model for human spinal researches? Morphometrical comparison study. Lab. Anim. Res. 29, 183–189. https://doi.org/10.5625/lar.2013.29.4.183.
Makanji, H., Schoenfeld, A.J., Bhalla, A., Bono, C.M., 2018. Critical analysis of trends in lumbar fusion for degenerative disorders revisited: influence of technique on fusion rate and clinical outcomes. Eur. Spine J. 27, 1868–1876. https://doi.org/10.1007/s00586-018-5544-x.
Malhotra, A., Pelletier, M.H., Yu, Y., Christou, C., Walsh, W.R., 2014. A Sheep Model for Cancellous Bone Healing. Front. Surg. 1, 1–7. https://doi.org/10.3389/fsurg.2014.00037.
Michalek, A.J., Funabashi, K.L., Iatridis, J.C., 2010. Needle puncture injury of the rat intervertebral disc affects torsional and compressive biomechanics differently. Eur. Spine J. 19, 2110–2116. https://doi.org/10.1007/s00586-010-1473-z.
Michalek, A.J., Iatridis, J.C., 2012. Height and torsional stiffness are most sensitive to annular injury in large animal intervertebral discs. Spine J. 12, 425–432. https://doi.org/10.1016/j.spinee.2012.04.001.
Mobbs, R.J., Phan, K., Malham, G., Seex, K., Rao, P.J., 2015. Lumbar interbody fusion: techniques, indications and comparison of interbody fusion options including PLIF, TLIF, MI-TLIF, OLIF/ATP, LLIF and ALIF. J Spine Surg 1, 2–18. https://doi.org/10.3978/j.issn.2414-469X.2015.10.05.
Mølster, A.O., 1984. Effects of rotational instability on healing of femoral osteotomies in the rat. Acta Orthop. Scand. 55, 632–636. https://doi.org/10.3109/17453678408992411.
Nagaraja, M.P., Risin, D., 2013. The current state of bone loss research: Data from spaceflight and microgravity simulators. J. Cell. Biochem. 114, 1001–1008. https://doi.org/10.1002/jcb.24454.
O'Connell, G.D., Vresilovic, E.J., Elliott, D.M., 2007. Comparison of animals used in disc research to human lumbar disc geometry. Spine (Phila. Pa. 1976). 32, 328–33. Doi: 10.1097/01.brs.0000253961.40910.c1.
Panjabi, M.M., 2003. Clinical spinal instability and low back pain. J. Electromyogr. Kinesiol. 13, 371–379. https://doi.org/10.1016/S1050-6411(03)00044-0.
Pearce, A.I., Richards, R.G., Milz, S., Schneider, E., Pearce, S.G., 2007. Animal models for implant biomaterial research in bone: A review. Eur. Cells Mater. 13, 1–10. https://doi.org/10.22203/eCM.v013a01.
Pintar, F.A., Yoganandan, N., Myers, T., Elhagediab, A., Sances, A., 1992. Biomechanical properties of human lumbar spine ligaments. J. Biomech. 25, 1351–1356.
Postigo, S., Schmidt, H., Rohlmann, A., Putzier, M., Simón, A., Duda, G., Checa, S., 2014. Investigation of different cage designs and mechano-regulation algorithms in the lumbar interbody fusion process - A finite element analysis. J. Biomech. 47, 1514–1519. https://doi.org/10.1016/j.jbiomech.2014.02.005.
Reitmaier, S., Schmidt, H., Ihler, R., Kocak, T., Graf, N., Ignatius, A., Wilke, H.-J., 2013. Preliminary investigations on intradiscal pressures during daily activities: an in vivo study using the merino sheep. PLoS One 8, e69610. https://doi.org/10.1371/journal.pone.0069610.
Reitmaier, S., Volkheimer, D., Berger-Roscher, N., Wilke, H.-J., Ignatius, A., 2014. Increase or decrease in stability after nucleotomy? Conflicting in vitro and in vivo results in the sheep model. J. r. Soc. Interface 11, 20140650. https://doi.org/10.1098/rsif.2014.0650.
Reitmaier, S., Schuelke, J., Schmidt, H., Volkheimer, D., Ignatius, A., Wilke, H.-J., 2017. Spinal fusion without instrumentation – Experimental animal study. Clin. Biomech. 46, 6–14. https://doi.org/10.1016/j.clinbiomech.2017.04.008.
Schmidt, H., Heuer, F., Simon, U., Kettler, A., Rohlmann, A., Claes, L., Wilke, H.-J., 2006. Application of a new calibration method for a three-dimensional finite element model of a human lumbar annulus fibrosus. Clin. Biomech. 21, 337–344. https://doi.org/10.1016/j.clinbiomech.2005.12.001.
Schmidt, H., Heuer, F., Drumm, J., Klezl, Z., Claes, L., Wilke, H.-J., 2007. Application of a calibration method provides more realistic results for a finite element model of a lumbar spinal segment. Clin. Biomech. 22, 377–384. https://doi.org/10.1016/j.clinbiomech.2006.11.008.
Shefelbine, S.J., Augat, P., Claes, L., Simon, U., 2005. Trabecular bone fracture healing simulation with finite element analysis and fuzzy logic. J. Biomech. 38, 2440–2450. https://doi.org/10.1016/j.jbiomech.2004.10.019.
Steiner, M., Claes, L., Ignatius, A., Simon, U., Wehner, T., 2014. Disadvantages of interfragmentary shear on fracture healing-mechanical insights through numerical simulation. J. Orthop. Res. 32, 865–872. https://doi.org/10.1002/jor.22617.
Tarpada, S.P., Morris, M.T., Burton, D.A., 2017. Spinal fusion surgery: A historical perspective. J. Orthop. 14, 134–136. https://doi.org/10.1016/j.jor.2016.10.029.
Uhthoff, H.K., Rahn, B.A., 1981. Healing patterns of metaphyseal fractures. Clin. Orthop. Relat. Res. 295–303.
Vergroesen, P.-P.-A., Kingma, I., Emanuel, K.S., Hoogendoorn, R.J.W., Welting, T.J., van Royen, B.J., van Dieën, J.H., Smit, T.H., 2015. Mechanics and biology in intervertebral disc degeneration: a vicious circle. Osteoarthr. Cartil. 23, 1057–1070. https://doi.org/10.1016/j.joca.2015.03.028.
Weinans, H., Huiskes, R., Grootenboer, H.J., 1992. The behavior of adaptive bone-remodeling simulation models. J. Biomech. 25, 1425–1441.
Zöllner, J., Heine, J., Eysel, P., 2000. Influence of nucleotomy to biomechanical behavior of lumbar motion segment Summary: Zentralbl. Neurochir. 61, 138–142. https://doi.org/10.1055/s-2000-10996.